Transactions, SMiRT-22
San Francisco, California, USA - August 18-23, 2013
Division X

SEISMIC BEHAVIOR AND DESIGN OF A PRIMARY SHIELD STRUCTURE CONSISTING OF SC WALLS

Peter N. Booth[1], Amit H. Varma[2], and Mitsubishi Heavy Industries[3]

[1] PhD Candidate, Dept. of Civil Engineering, Purdue University, W. Lafayette, IN (boothpn@purdue.edu)
[2] Associate Professor, Dept. of Civil Engineering, Purdue University, W. Lafayette, IN
[3] Mitsubishi Heavy Industries, LTD, Kobe, Japan.

ABSTRACT

This paper presents the results of a study on the seismic behavior and design of a unique primary shield wall (PSW) structure designed for a typical pressurized water reactor (PWR) nuclear power plant. The PSW structure is composed of steel-plate reinforced concrete composite (SC) walls with three steel plates (two on the interior and exterior surfaces and one in the middle) for reinforcement. Researchers in Japan have tested a 1/6th scale physical model of the PSW structure (consisting of SC walls) to determine its lateral load-deformation behavior (Shodo et al. 2003). This paper presents the development and benchmarking of a nonlinear inelastic finite element (NIFE) modeling and analysis approach for predicting the lateral load-deformation behavior of the 1/6th scale physical model of PSW structure. The analysis results are compared with experimental observations, and used to gain additional insight into the lateral load-deformation behavior of the PSW structure. This additional insight is used to develop a simpler design approach for calculating the lateral load capacity of the PSW structure. The experimental and analytical results indicate that the lateral load capacity of the tested PSW structure depends on the shear strength of the SC walls that constitute the PSW structure.

INTRODUCTION

The design of nuclear power plant structures provides a unique set of challenges and conditions in comparison to typical commercial building structures. The extensive use of SC structures in the current generation of nuclear power plants is due to a combination of factors such as accelerated construction, improved quality control, and desirable structural properties. Research in the last few years has shown that SC structures can also be used more efficiently than reinforced concrete structures in safety-related nuclear facilities. Research has also shown that SC structures perform well for a wide range of structural loading conditions such as seismic loading (Varma, Zhang et al. 2011), thermal-mechanical loading (Varma, Malushte et al. 2011), and blast loading (Mizuno et al. 2005).

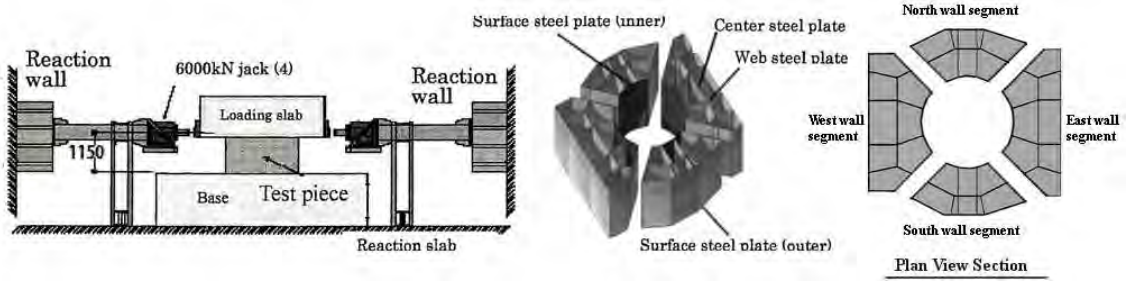

Figure 1. Experimental test setup and cross-section of SC primary shield (Shodo et al. 2003)

This paper investigates the seismic behavior and design of a primary shield wall (PSW) structure that is part of a typical PWR nuclear power plant design. The PSW structure is typically a very thick, massive, and geometrically complex structure. Figure 1 shows an isometric view of a cross-section going

through the PSW structure with concrete removed. As shown, the PSW is a hollow polygonal structure with steel plates on the interior and exterior surfaces, and an additional steel plate at the mid-thickness. These three steel plates of each SC wall are connected to each other by transverse (web) steel plates that are welded to the steel plates. The steel plates are anchored to the concrete infill with sufficient shear studs to generate adequate composite action and prevent local buckling of the steel surface plates. Additionally, there are four openings (shown in the plan view in Figure 1) in the PSW structure that reduce connectivity and interaction, and separate the PSW structure into four SC wall segments further adding to the complexity.

Researchers in Japan have tested a 1/6th scale physical model of this PSW structure consisting of composite SC walls. The results of these experimental investigations were presented by Shodo et al. (2003). Figure 1 includes an elevation view of the test setup. As shown in the test setup, the concrete base is rigidly connected to the reaction slab and the specimen is free-standing. Lateral loading is applied to the concrete block on top of the specimen with hydraulic actuators. The results from the lateral loading test are presented in Shodo et al. (2003), and not repeated here for brevity.

This paper focuses on the development and benchmarking of a NIFE modeling and analysis approach that can be used to predict the lateral load-deformation response of the tested 1/6th scale model PSW structure, and to gain additional insight into its behavior. The results from the experimental and analytical investigations are then used to develop a simpler design approach that is based on conventional approaches combined with the understanding of behavior and principles of structural mechanics.

SUMMARY OF NIFE MODEL OF PSW STRUCTURE

A 3D finite element model of the 1/6th scale test specimen of the PSW structure was developed and analysed using ABAQUS (2012). The model explicitly accounts for all the steel plates (interior and exterior surface plates, and the mid thickness plate), and the web plates. These plates are modeled using 4-node S4R shell elements with reduced integration. The concrete infill is modeled using eight node C3D8R elements with reduced integration. The shear studs providing bond interaction and composite action between the steel plates and the concrete infill were also modeled explicitly using nonlinear spring (connector) elements. The details of the material models used for the steel and concrete materials, and the force-deformation relationship for the connector elements are summarized in the following sub-sections. The finite element model was analyzed using a quasi-static explicit analysis procedure to include the complexities of material and geometric nonlinear, inelastic, and interaction behavior.

Concrete and Steel Material Modeling

The concrete elastic fracture (CEF) model in ABAQUS (2012) is used for the modeling the concrete elements. The CEF model is a suitable option for this analysis since the behavior is dominated by the effects of Mode I and Mode II fracture, shear retention, anisotropic damage evolution, and accurate simulation of simultaneous shear retention and diagonal concrete compression.

The CEF model assumes linear elastic behavior for the concrete in compression. The linear compression model is reasonable if the global structural behavior of concrete is dominated by brittle cracking, tension softening and shear retention. In the case of the 1/6th scale PSW structure, the large amount of steel plate area (reinforcement ratio) resists compression in combination with concrete thus reducing the overall compression demand of the concrete section. Additionally, the cellular-like geometry of the steel section provides substantial confinement of concrete in compression zones thus increasing the compression stiffness and strength.

The tension behavior of the concrete is governed by a Rankine criterion for the detection of initial cracking. After the initiation of cracking, the CEF model fixes the crack orientation for the duration of the analysis. If subsequent cracking occurs at the same integration point, the subsequent crack orientations are orthogonal to the initial crack direction and also fixed for the duration of the analysis.

The steel is modeled using multi-axial plasticity theory with: (i) von Mises yield surface, (ii) associated flow rule, and (iii) isotropic hardening. The idealized steel uniaxial stress-strain (σ–ε) curve is

shown in Figure 2. The uniaxial stress-strain curve consists of a linear elastic portion, post-yield plateau region, and strain-hardening region. The parameters used to define the idealized stress-strain curve are: (i) elastic modulus E, (ii) yield stress σ_y, (iii) yield strain ε_y (iv) yield plateau length $m\varepsilon_y$, (v) strain corresponding to onset of strain hardening ε_{sh}, (vi) ultimate stress σ_u, and (vii) strain corresponding to ultimate stress ε_u. Equation 1 defines the stress-strain behavior in the strain hardening region of the response. The idealized stress-strain curve shown is converted into a true stress-true plastic strain (σ–ε_p) so that large deformation and large strain behavior can be correctly modeled in the analysis.

$$\sigma = \sigma_u - (\sigma_u - \sigma_y) \times \left(\frac{\varepsilon_u - \varepsilon}{\varepsilon_u - \varepsilon_{sh}} \right)^n \tag{1}$$

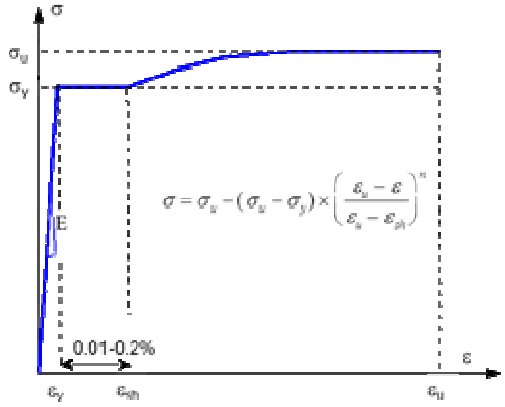

Figure 2. Idealized Stress-Strain Curve for Steel Plates.

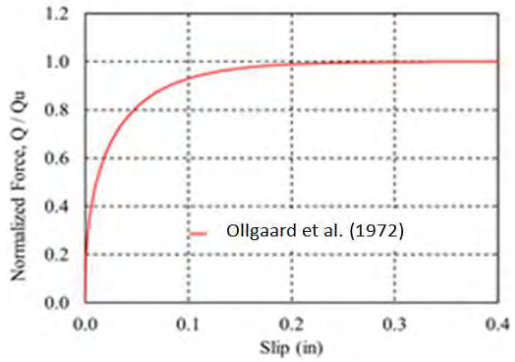

Figure 3. Stud Force vs. slip relationship used for the connector elements

Shear Stud Modeling and Composite Behavior

The shear studs between the steel plates and concrete infill were modeled using nonlinear spring (connector) elements. These connector elements were defined by: (i) connecting the coincident steel plate and concrete infill nodes at the locations of the shear studs in the actual structure, and (ii) specifying the force-displacement relationships for the connected degrees of freedom. The shear stud force-displacement (slip) behavior developed by Ollgaard et al. (1972) was specified as the force-displacement behavior for the connector element degrees of freedom corresponding to interfacial slip between the steel plates and the concrete infill. Figure 3 shows the shear stud force-displacement (Q-Δ) relationship that was developed using Equations 2 and 3 provided by Ollgaard et al. (1972), where the stud strength (Q_u) and stiffness are functions of the stud cross-sectional area (A_{stud}), concrete compressive strength (f'_c), elastic modulus of concrete (E_c), and the ultimate strength of the stud ($F_{u,\,stud}$):

$$Q = Q_u (1 - e^{-18\Delta})^{2/5} \tag{2}$$

$$Q_u = \min(\phi A_{stud} F_{u,stud}, 0.5 A_{stud} \sqrt{f'_c E_c}) \tag{3}$$

Boundary Conditions and Meshing

Mesh sizes and distributions for the concrete and steel part instances are shown in Figure 4. The solid concrete elements are 8-node linear reduced integration brick elements with an average size of 3 inches. The steel elements are 4-node doubly curved thick shell elements with reduced integration, enhanced hourglass control, and finite membrane strains. The average size of the steel elements is 2 inches by 2 inches. Simpson integration rule is used for the steel shell elements with 5 integration points specified through the thickness of the elements. These shell elements are capable of capturing the nonlinear section stresses and strains and local buckling.

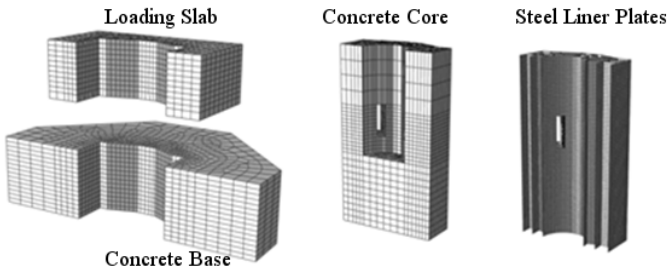

Figure 4. Detailed View of FEM Model and Meshing

Analysis Method and Loading Protocol

The finite element analyses were conducted using the explicit dynamic (quasi-static) analysis approach in ABAQUS (2012). The explicit dynamic analysis approach was used because of significant material nonlinearities (concrete cracking) and complex interactions between the model components at and beyond peak load capacity. Both monotonic and cyclic lateral loading analyses were conducted by applying lateral loading to the upper concrete block as shown in Figure 1. The monotonic analysis was conducted by applying lateral loading (pushing) up to the target displacement from the experiment. The cyclic analyses were conducted by applying lateral loading in accordance with the experimental cyclic loading history.

SUMMARY OF ANALYSIS RESULTS AND BEHAVIOR

Figure 5 compares the results from the NIFE analyses with the experimental lateral load-displacement responses. It includes the results from the monotonic analysis and its comparisons with the envelope of the cyclic lateral load-displacement responses. As shown, the NIFE analysis results compare favorably with the experimental response. Additionally, Figure 5 shows excellent correlation between the cyclic lateral load-displacement responses predicted analytically and those measured experimentally. Thus, the NIFE modeling and analysis approach for the complex PSW structure consisting of unique SC walls is benchmarked by using the results from the 1/6th scale test conducted by Shodo et al. (2003).

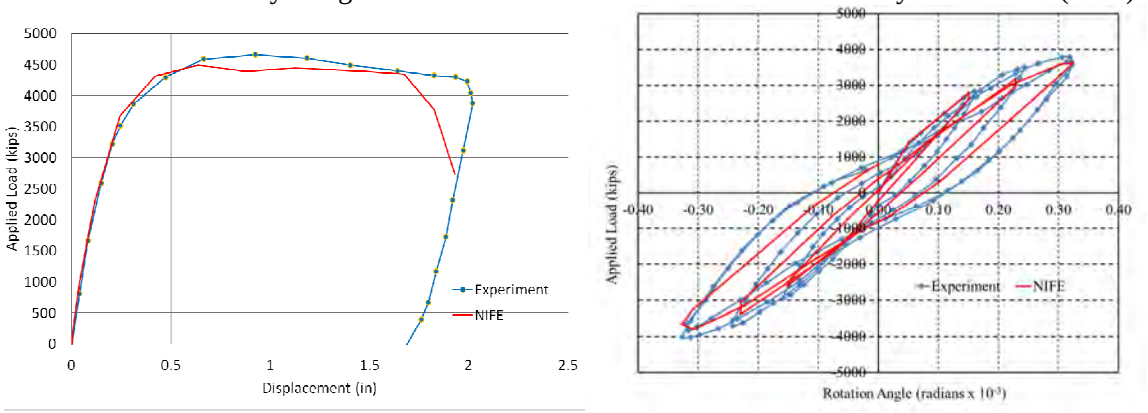

Figure 5. Monotonic and Cyclic Load Displacement Curves

Figures 6, 7, and 8 and Table 2 provide additional insights into the lateral load behavior of the PSW structure and further compare the analysis results with experimental measurements and observations. Figure 6 shows the progression of yielding of the steel plates (interior and exterior surface and mid-thickness) of the PSW structure. The figure shows contour plots of the von Mises stresses in the steel plates at lateral loads equal to 1000, 2000, 3000, and 4000 kips. The contour plots are limited to the maximum value corresponding to the yield stress of the steel plates, and all portions with red color are

fully yielded. Figure 6 shows that the exterior (outer) steel plate yields at about 3000 kips on the tension side (according to the overturning moment). The middle steel plate also yields at about 3000 kips in the middle segment. At 4000 kips of lateral load all the steel plates (outer, inner, and middle) have undergone significant yielding. These von Mises stress contour plots indicate that all three steel plates participate in the lateral load resisting mechanism, which is an important finding for the complex PSW structure consisting of SC walls with three steel plates.

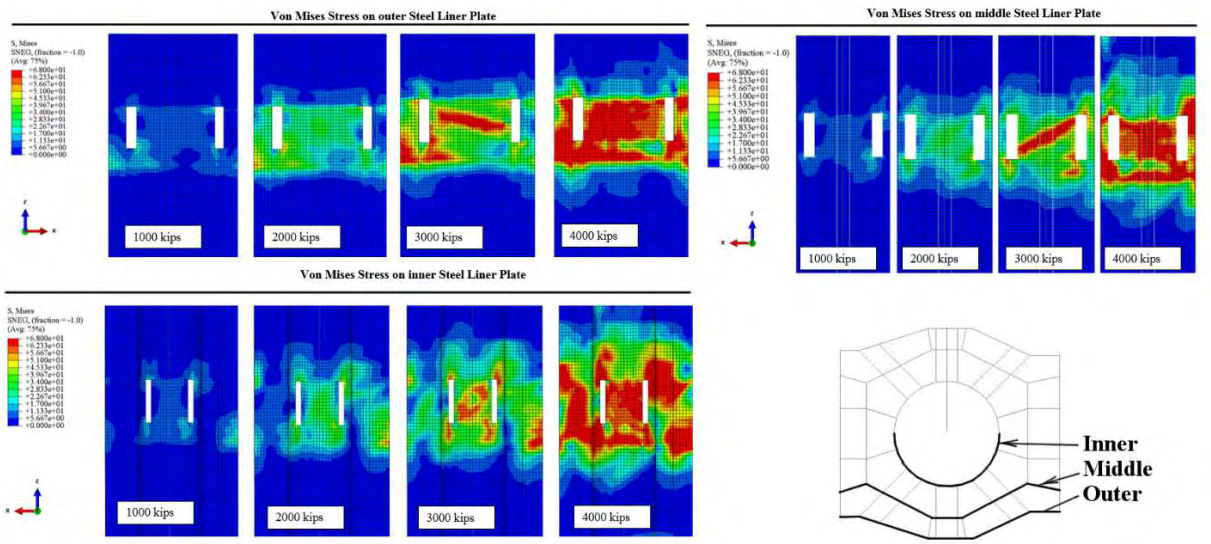

Figure 6. Von Mises Stresses in outer, middle, and inner steel plates

As mentioned earlier and shown in Figure 1, the PSW structure is separated into four SC wall segments. Each of these SC wall segments has three steel plates (outer surface, inner surface, and mid-thickness) and several web plates. The four SC wall segments are referred as end segments and middle segments for the rest of this discussion. The two end segments are subjected: (i) shear due to the applied lateral loading, and (ii) axial tension or compression due to the overturning moment. The two middle segments are subjected primarily to longitudinal shear due to the applied lateral loading.

Figures 7 and 8 show the progression of concrete cracking and the formation of concrete compression struts in the SC wall segments. Figure 7 shows the magnitude and directions of the minimum principle stresses (compression struts) in the concrete infill of the SC wall segments. The left side of Figure 7 focuses on the middle segments, and the right side focuses on the end segments. As shown, all the SC wall segments develop concrete compression struts and participate in carrying the applied lateral load in shear. This is an important finding for the complex PSW structure consisting of SC wall segments. As the lateral load exceeds 3000 kips, the compression struts in the middle segments exhibit reduction in their stress carrying ability due to excessive diagonal tension cracking (see Figure 8 discussion below), and subsequently the end wall segments resist a larger portion of the applied lateral load.

Figure 8 shows the magnitudes and directions of the maximum principal strains (cracking strains) in the concrete infill of the SC wall segments. The left side of Figure 8 focuses on the middle segments, and the right side focuses on the end segments. As shown, diagonal tension cracking occurs in the middle segment at lateral load level of 2000 kips. This diagonal tension cracking becomes extensive as the lateral load exceeds 3000 kips. In the end wall segments, tension cracking occurs in the end wall segment subjected to axial tension due to the overturning moment. However, the end wall segment subjected to axial compression due to the overturning moment does not experience significant cracking for low load levels (less than 2000 kips). As the lateral load level increases and exceeds 3000 kips, the end wall segments exhibit more diagonal tension cracking. This occurs after the middle wall segment exhibits reduction in its stress carrying ability (softening), and the end segments resist larger portions of the applied lateral load. As shown in Figures 7 and 8, the end wall segments exhibit significant diagonal

tension cracking and reduction in their compression strut stress carrying ability as the lateral load exceeds 4000 kips. Thus, all the four SC wall segments contribute significantly to the lateral load carrying capacity of the complex PSW structure, which is an important finding.

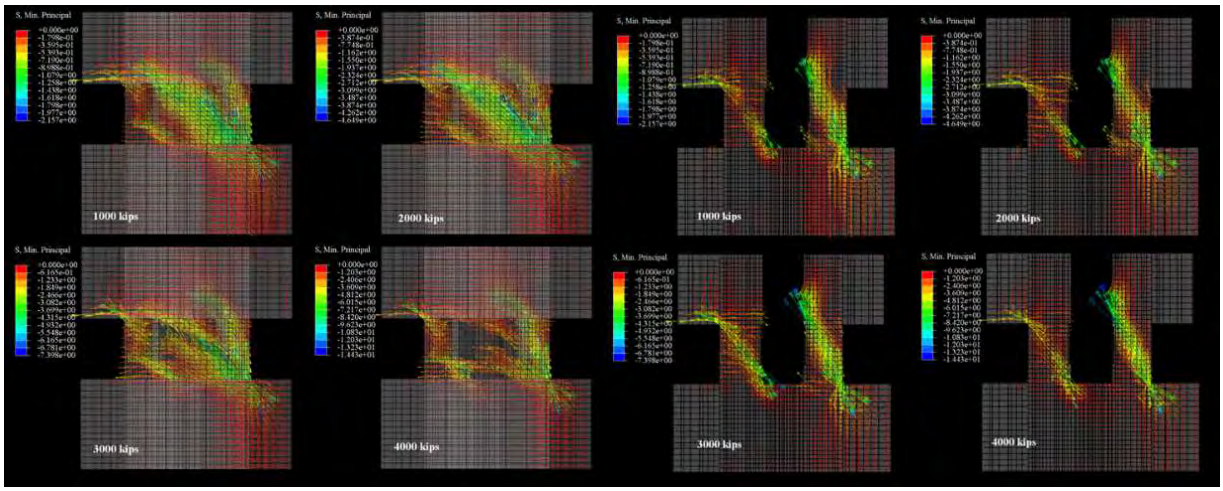

Figure 7. Concrete Minimum Principle Stress (Compression Strut) in Middle and End Wall Segments

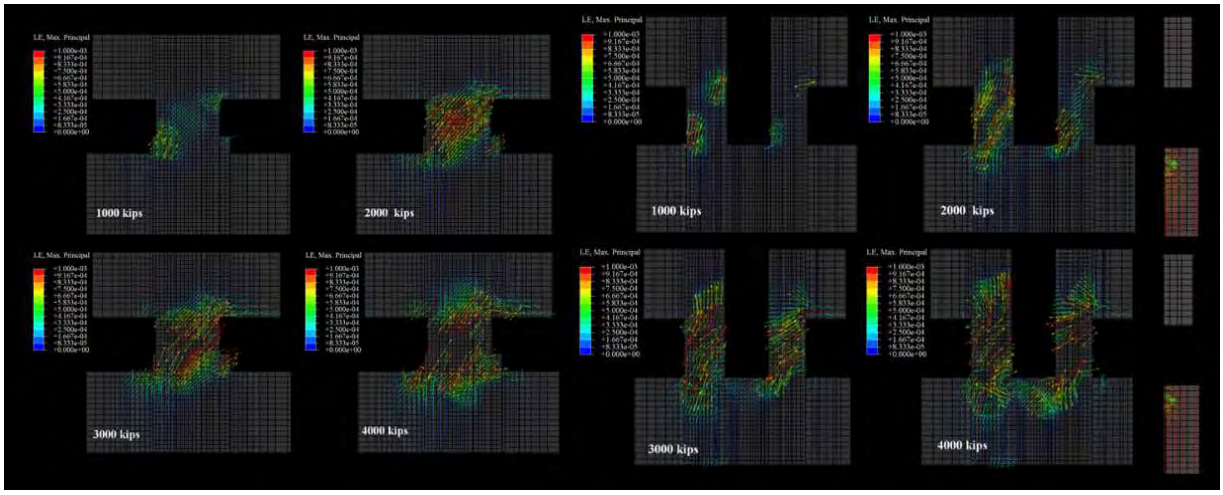

Figure 8. Concrete Maximum Principle Strain (Cracking Strain) in Middle and End Wall Segments

Figure 9 and Table 2 compare the lateral load-deformation behavior of the 1/6th scale test and the NIFE analysis of the PSW structure. Key milestones in the loading progression are identified and compared in both Figure 9 and Table 2. As shown, flexural tension cracking of the concrete in the tension end wall segment occurs at a lateral force level of approximately 750 kips. First yield of the outer (exterior) steel plate of the end wall segment on the tension side occurs at approximately 2500 kips. Shear yielding of the outer (exterior) steel plate of the middle wall segment occurs at a lateral force level of approximately 3000 kips. The graphical and numerical comparisons in Figure 9 and Table 2 confirm that the NIFE analysis results compare favorably and conservatively with the experimental results. This benchmarks the NIFE modeling and analysis approach for predicting lateral load behavior of the complex PSW structure.

Table 2: Numerical Comparison of Experiment and NIFEAnalysis Results

Event	Lateral Load from Experiment Shodo et al. (2003)	Lateral Load from NIFE analysis
(A) Flexural Tension Concrete Cracking in End Wall Segment	560 kips	750 kips
(B) Flexural Tension Yielding of Outer Steel Plate in End Wall Segment	2700 kips	2500 kips
(C) Shear Yielding of Steel Plate in Middle Wall Segment	3060 kips	3000 kips

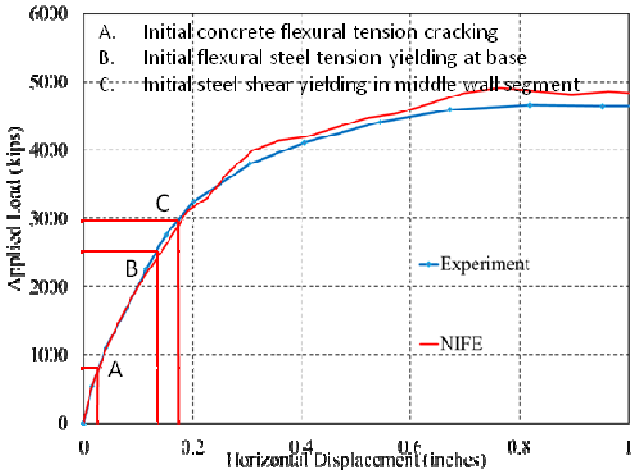

Figure 9 Comparison of Experimental and NIFE Analysis Behavior

DESIGN LATERAL LOAD CAPACITY

The results from the benchmarked NIFE analyses indicate that all four SC wall segments (two end wall and two middle wall segments) participate and contribute to the lateral load capacity of the complex PSW structure. The analysis results further indicate that the SC wall segments: (i) develop diagonal tension cracking and compression struts in the concrete infill, and (ii) von Mises yielding of all three (outer, inner, and middle) steel plates. Thus, all the SC wall segments resist the applied lateral loading in shear.

The relative distribution of the lateral load resisted by the individual SC wall segments is shown in Figure 10. Figure 10 shows the portion of the base shear resisted by the individual SC wall segments. The plot on the left of Figure 10 shows the results from the NIFE analysis, while the plot on the right shows the results from an equivalent linear elastic finite element (LEFE) analysis. The LEFE analysis was conducted using linear elastic material models for the steel and concrete materials and assuming full bond between the steel plates and the concrete. As shown by the NIFE analysis results, the wall segments resisted equal portions (approximately 25%) of the total base shear up to 0.4 in. lateral displacement, which corresponds to an applied lateral load of 4000 kips (see Figure 9). After 0.4 in. lateral displacement, the portion of the base shear resisted by the middle segment reduces due to reasons explained earlier, and the portions of the base shear resisted by the end segments increases. The results of the LEFE analysis cannot account for this behavior due to its modeling limitations, but it also indicates that each SC wall segment resists 20-30% of the total base shear. This is an important finding because it

indicates that LEFE analysis results can also be used to estimate the portions of the base shear resisted by the individual SC wall segments.

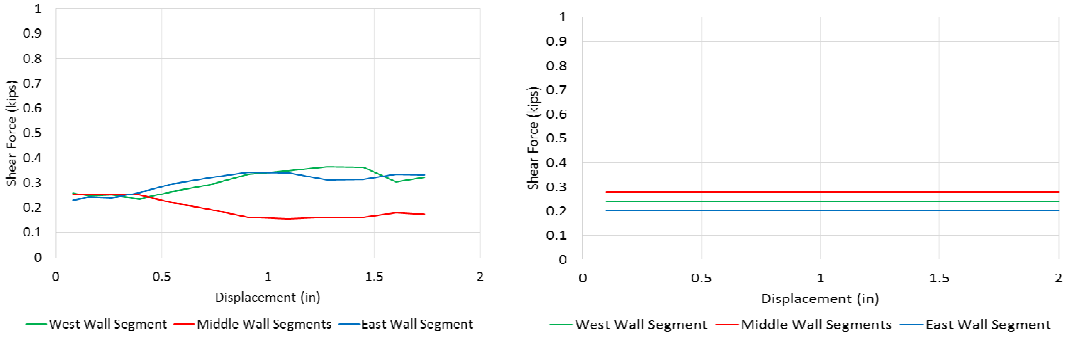

Figure 10. Comparison of Normalized Shear Resistance of Wall Segments

The lateral load capacity of the PSW structure can be calculated by adding the shear strengths of the individual SC wall segments. This is a reasonable design assumption based on the behavioral insight described above, namely, all SC wall segments contribute almost equally to the lateral load capacity of the PSW structure.

The NIFE analysis results show that the behavior of the SC wall segments is comparable to that of reinforced concrete squat shear walls. This is based on the formation of diagonal tension cracks and compression struts in the concrete, and von Mises yielding of shear reinforcement (steel plates) in the SC wall segments. This behavioral insight leads to an additional design assumption that the shear strength of the four individual wall segments can be calculated using the ACI 349-06 code provisions for the in-plane shear strength of RC walls.

$$V_n = A_{cv}\left(\alpha_c \sqrt{f'_c} + \rho_t f_y\right) \tag{2}$$

$$\alpha_c = 3.0 \ for \ \frac{h_w}{l_w} \le 1.5 \tag{3}$$

$$\alpha_c = 2.0 \ for \ \frac{h_w}{l_w} \ge 2.0 \tag{4}$$

The relevant ACI 349-06 code provisions are summarized in Equations (2) – (4). In these Equations A_{cv}, f'_c, ρ_t, and f_y are the area of the concrete, compressive strength, transverse steel reinforcement ratio, and steel yield strength, respectively. As shown, the in-plane shear strength is the sum of the shear strength contributions of the concrete and the shear reinforcement. The concrete contribution to the shear strength depends on the wall aspect ratio (wall height divided by length, h_w/l_w).

The ACI 349-06 code equations were used for each of the SC wall segments. The concrete area (A_{cv}) and the aspect ratios were based on the geometric details of each wall segment. As shown in Figure 12, the steel shear reinforcement area was calculated as the summation of the areas of individual steel plates that are almost (approximately) parallel to the direction of the applied loading.

The total lateral load capacity of the PSW structure (V_n) was calculated as the sum of the shear strengths of the individual SC wall segments to be equal to 4500 kips. The shear strength contributions of the each end segment and middle segment were equal to 30% and 20%, respectively, of the total lateral load capacity. Figure 12 includes the comparison of the calculated lateral load capacity with the NIFE analysis results and the experimental results. As shown, the calculated lateral load capacity compares favorably and conservatively with these results.

ACI 349-06 also limits (provides an upper bound for) the in-plane shear strength of RC walls that are part of a lateral load resisting system to $8(f'_c)^{0.5}A_{cv}$. As shown in Figure 12, this limit is extremely conservative, and it does not apply to the PSW structure composed of SC walls.

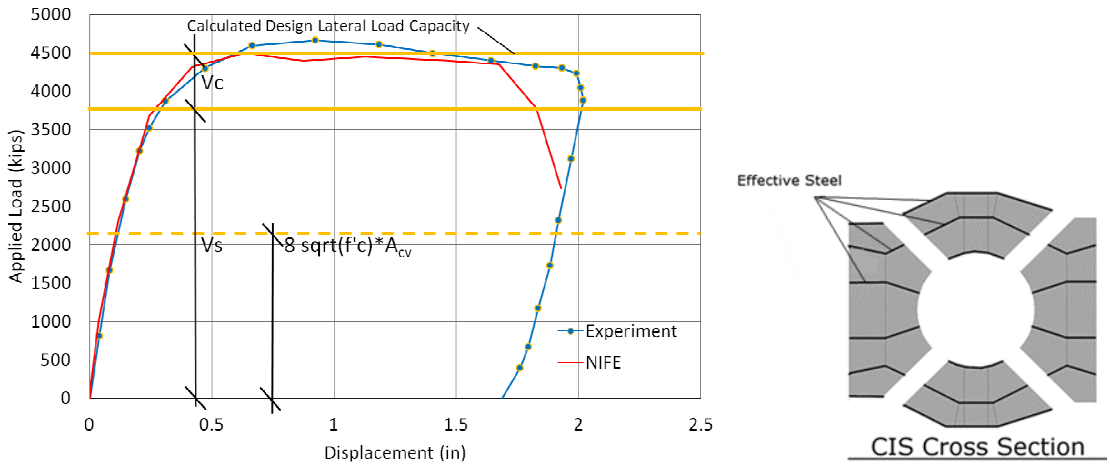

Figure 12. Design Shear Strength and Section Properties for Calculation of Shear Strengths

The overturning moment (M_{OTM}) at base of the PSW structure corresponding to the lateral load capacity (V_n) can be calculated as V_n multiplied by the height of the specimen. This total overturning moment is resisted by: (i) each of the four SC wall segments, and (ii) the two end segments by developing an axial force couple as shown in Figure 13. The results from the NIFE analysis and the LEFE analyses were further post-processed to identify the portions of the overturning moment resisted by the four wall segments, and the portion resisted by the axial force couple in the end wall segments.

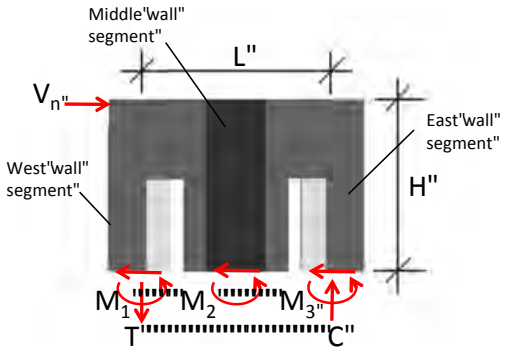

$M_{OTM}=V_nH=M_1+M_2+M_3+(T+C)e/2$
where,
M_{OTM} = Total overturning moment
M1, M3 = moment resisted by end segments
M2 = moment resisted by middle segment
T, C = axial force couple in end segments for resisting M_{OTM}

Figure 13. Overturning Moments Resisted by the PSW Structure and Wall Segments

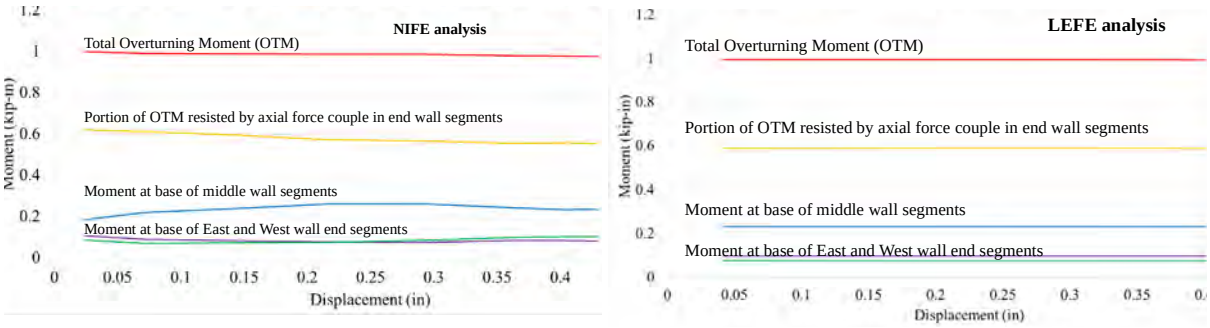

Figure 14. Portions of the Overturning Moment Resisted by the PSW Wall Segments

Figure 14 presents the results from this post-processing of the NIFE and LEFE analyses. As shown, the axial force couple in the end wall segments resists about 60% of the overturning moment. Additionally, the two middle wall segments resist approximately 25% of the overturning moment, and the

two end segments resist approximately 15% of the overturning moment. These results are reasonably consistent between the NIFE and LEFE analysis results. This is an important finding because it indicates that LEFE analysis results can also be used to estimate the portions of the overturning moments resisted by the individual SC wall segments and the axial force couple in the end segments.

The axial force (P_r) and bending moment (M_r) demands at the base of each wall segment associated with the total overturning moment ($M_{OTM} = V_n H$) can be calculated using the distributions and proportions described above. Additionally, axial force-bending moment capacity interaction curves can be developed for each SC wall segment by conducting section fiber analysis while using rigid-plastic material models for the steel and concrete. This approach for calculating axial force-bending moment capacity interaction curves has been used extensively for composite sections including concrete filled tubes and reinforced concrete sections (Mahin and Bertero 1977).

The resulting capacity interaction curves for each of the wall segments are shown in Figure 15. Additionally, the figure includes the data points corresponding to the axial force and moment demands (P_r and M_r) calculated at the base of each wall segment. As shown, all the data points lie within the corresponding interaction curves, which means that none of the SC wall segments will fail individually in flexure due to the overturning moment (M_{OTM}) associated with lateral load capacity (V_n) of the PSW structure. All the SC wall segments will fail in shear, and the lateral load capacity (V_n) of the PSW structure can be calculated as the sum of the shear strengths of the individual SC wall segments.

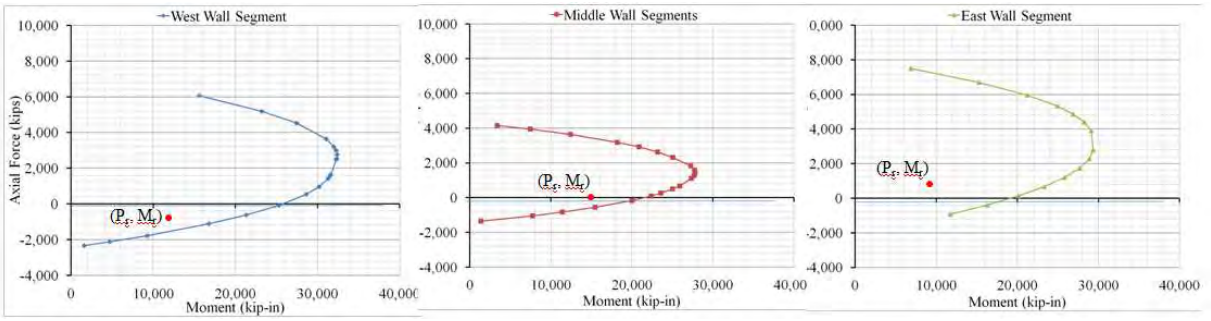

Figure 15. Axial Load-Bending Moment Capacity Interaction Curve for SC Wall Segments

CONCLUSIONS

The nonlinear inelastic finite element (NIFE) modeling and analysis approach presented in this paper was benchmarked for predicting the lateral load-deformation behavior of a complex primary shield wall (PSW) structure consisting of SC wall segments with three steel plates (interior and exterior surface, and mid-thickness steel plates).

The NIFE model predicted with reasonable accuracy the cyclic and monotonic lateral load-deformation behavior of the 1/6th scale test of the PSW structure. It also predicted with reasonable accuracy the key events that occurred along the load-deformation path, namely, the flexural tension cracking of the concrete, flexural tension yielding of the steel plates, and the shear yielding of the steel plates.

The NIFE model analysis also provided significant insights into the fundamental behavior of the SC wall segments of the PSW structure including the occurrence of diagonal tension cracking, the formation of concrete compression struts, and the von Mises yielding of all the three (interior, exterior, and mid-thickness) steel plates of each SC wall segment. The NIFE model analysis results indicate that the shear strength of the SC wall segments governs the behavior and strength of the PSW structure.

The insights from the NIFE analysis results were used to develop a simple approach for calculating the lateral load capacity (V_n) of the PSW structure by adding the shear strength of the individual SC wall segments. The ACI 349-06 code provisions were used to calculate the shear strength

of the individual SC wall segments. This design approach was shown to estimate the lateral load capacity of the PSW structure with reasonable accuracy.

REFERENCES

ABAQUS (2011). *ABAQUS/Standard Version 6.10 User's Manuals: Volume I-III*, Hibbitt, Karlsson, and Sorenson Inc., Pawtucket, RI.

ACI 349 (2006), "Code Requirements for Nuclear Safety-Related Concrete Structures and Commentary," American Concrete Institute, Farmington Hills, MI.

JEAG 4618 (2005). "Technical Guidelines for Seismic Design of Steel Plate Reinforced Concrete Structures: Buildings and Structures," Japanese Electric Association Nuclear Standards Committee, Tokyo, Japan

Mahin, S. A. and Bertero. V. V. (1977). *RCCOLA: A Computer Program for R. C. Column Analysis: User's Manual and Documentation*, Department of Civil Engineering, University of California, Berkeley, CA.

Mizuno, J., Koshika, N., Sawamoto, Y., Niwa, N., Yamashita, T., Suzuki, A., (2005). "Investigations on Impact Resistance of Steel Plate Reinforced Concrete Barriers against Aircraft Impact Part 1: Test Program and Results", Transactions of the 18th International Conference on Structural Mechanics in Reactor Technology (SMiRT-18), Vol. J J05/1.

Ollgaard, J.G., R. G. Slutter, and J.W. Fisher. Shear Strength of Stud Connectors in Lightweight and Normal-weight Concrete, Engineering Journal - American Institute of Steel Construction, 1972.

Shodo, A., K. Asao, O. Tetsuya, S. Kunihiko, and T. Kazuaki (2003) "A Study on the Structural Performance of SC Thick Walls", Annual Conference of Architectural Institute of Japan.

Varma, A.H., Zhang, K., Chi, H., Booth, P.N., and Baker, T. (2011) "In-Plane Shear Behavior of SC Composite Walls: Theory vs. Experiment." Transactions of the 21st SMiRT Conference, New Delhi, India, Paper ID 764, IASMiRT, North Carolina State University, Raleigh, NC.

Varma, A.H., Malushte, S.R., Sener, K., Booth, P.N., and Coogler, K. (2011). "Steel-Plate Composite Walls: Analysis and Design Including Thermal Effects." Transactions of the 21st SMiRT Conference, New Delhi, India, Paper ID 761, IASMiRT, North Carolina State University, Raleigh, NC.